Zero-Shot Self-Supervised Joint Temporal Image and Sensitivity Map Reconstruction via Subspace Model

Author name(s) withheld EMAIL(S) WITHHELD
Address withheld

Editors: Under Review for MIDL 2023

Abstract

Fast spin-echo (FSE) pulse sequences for Magnetic Resonance Imaging (MRI) offer important imaging contrast in clinically feasible scan times. For further acceleration, self-supervised learning via data undersampling (SSDU) achieves high-fidelity reconstructions from undersampled data by learning a regularization function without a standard supervised training data set. On the other hand, T2-shuffling resolves temporal signal dynamics in FSE acquisitions by exploiting temporal correlations via a linear subspace model. In this work, we propose a novel approach that incorporates the temporal subspace model into the SSDU framework to improve time-resolved FSE reconstruction quality. Additionally, in regimes without pre-acquired sensitivity maps, we propose joint estimation of coil-sensitivity maps using an iterative reconstruction technique. In addition, our technique functions in a zero-shot fashion, as it only utilizes data from the single scan it aims to reconstruct. We perform experiments on simulated and retrospective in-vivo data to evaluate the performance of the proposed zero-shot learning method for temporal FSE reconstruction. The results demonstrate the success of our proposed method where NMSE and SSIM are significantly increased and the artifacts are reduced.

Keywords: Temporal MR image reconstruction, Subspace signal model, Zero-shot supervised learning, Joint sensitivity map estimation.

1. Introduction

Fast spin-echo (FSE) Magnetic Resonance Imaging (MRI) sequences provide a variety of image contrasts at different echo times in clinically reasonable scan times (Hennig et al., 1986; Mugler III, 2014). While standard FSE reconstructs a single image, recent techniques aim to resolve a time-series of images during each echo of a FSE acquisition.

T2-shuffling has demonstrated success in resolving temporal images from volumetric FSE acquisitions (Tamir et al., 2017; Bao et al., 2017; Iyer et al., 2021). T2 shuffling randomly shuffles the phase encode view ordering, exploits temporal correlations with a low-dimensional subspace model, and utilizes a predefined regularization (Lustig et al., 2008; Zhao et al., 2015). However, limited achievable incoherence in 2D-acquisition precludes widespread use of T2-shuffling in 2D FSE acquisitions.

Recently, deep learning (DL) has gained interest for high-quality accelerated MRI by combining data consistency and a learned regularization from deep neural networks in an unrolled manner (MoDL) (Aggarwal et al., 2018). However, MoDL requires a large scale training dataset of under-sampled data with associated ground truth, which may be unrealistic to acquire in clinical practice. To train models without ground truth, Yaman et al. (Yaman et al., 2020b,a, 2021) proposed a self-supervised learning reconstruction method

© 2023 Anonymous.

(SSDU), which trains models in a self-supervised fashion by partitioning under-sampled kspace data into two disjoint sets, Θ and Λ, and training a network to predict Λ with the information from Θ.

Moreover, current reconstruction methods require pre-acquired coil sensitivity maps, usually estimated from fully sampled calibration regions (ESPIRIT) (Uecker et al., 2014). To further shorten total acquisition times or to handle scenarios with no calibration data available, joint reconstruction approaches are proposed to estimate coil sensitivity maps and in the unrolled iterative reconstruction of MRI (Jun et al., 2021; Arvinte et al., 2021).

Here, we propose a novel zero-shot self-supervised learning technique that jointly reconstructs coil sensitivity maps and a time-series of images from a single T2-shuffling acquisition by incorporating the subspace model into the SSDU framework. Our contributions are the following: 1) We train our model in a zero-shot, self-supervised fashion from just a single under-sampled 2D T2-shuffling acquisition. 2) We incorporate the temporal signal subspace model into the existing SSDU framework along with random masking to mitigate over fitting. 3) Our zero-shot self-supervised framework jointly estimates coil sensitivity maps and the time-series of images. We demonstrate the success of our model on both simulated data and in-vivo scanning data with different sampling patterns. The overall image qualities are significantly improved.

2. Methods

2.1. Linear temporal subspace model

Strong correlation exists amongst temporal signal evolution of FSE sequences from tissues with differing (T2, T1) tissue parameters. Thus, a linear low-rank approximation of the signal correlation will help reduce the degrees of freedom in the time-resolved reconstruction problem (Tamir et al., 2017).

FSE signal evolution can be simulated with the Extended Phase Graph (EPG) (Hennig, 1988; Ben-Eliezer et al., 2015) algorithm for a certain (T2, T1) and flip angle. A dictionary containing an ensemble of signal evolution from a range of (T2, T1) values and the flip angle of interest is generated. As depicted in Fig. 1(a), taking the first K singular vectors of the simulated dictionary produces a linear subspace model $\mathbf{\Phi} \in \mathbb{C}^{T\times K}$, where T is the number of echos, which more compactly represents FSE signal evolution.

By constraining the time-series of images to the subspace, $\mathbf{X_T} = \mathbf{\Phi}\boldsymbol{\alpha}$, where $\mathbf{X_T} \in \mathbb{C}^{T\times W\times H}$ are the pixels in the temporal images and $\boldsymbol{\alpha} \in \mathbb{C}^{K\times W\times H}$ are coefficients, the reconstruction directly solves for the low-dimensional coefficients:

$$\min_{\boldsymbol{\alpha}} \|\mathbf{Y} - \mathbf{MFS\Phi}\boldsymbol{\alpha}\|_2^2 + \mu R(\boldsymbol{\alpha}) \tag{1}$$

where $\mathbf{Y}$ is the acquired data, $\mathbf{M}$ is the sampling pattern, $\mathbf{F}$ is the Fourier transform, $\mathbf{S}$ is the sensitivity map and R is a regularization term.

2.2. Self-supervised image reconstruction framework

The self-supervised framework learns the regularization directly from the acquired, under-sampled data, without prior knowledge or ground truth, and combines the learned reg-

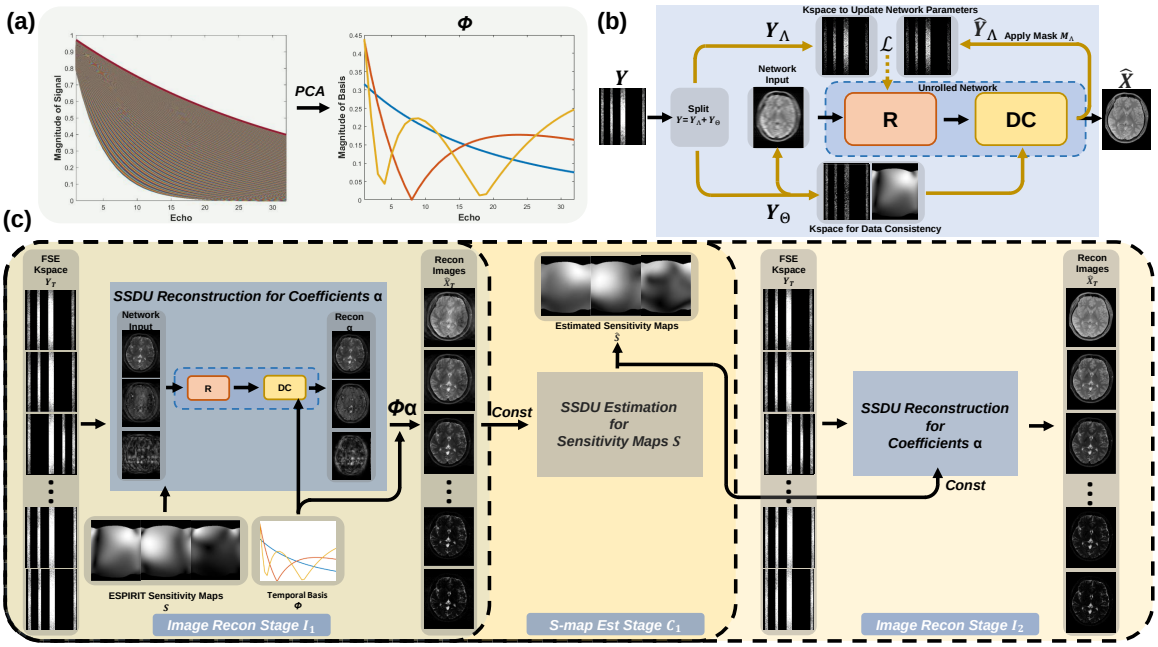

Figure 1: An overview of our proposed reconstruction framework. **(a)**: The temporal subspace model is generated by performing PCA on a signal evolution dictionary matrix and selecting the eigenvectors with the top K largest eigenvalues. **(b)**: The illustration of the SSDU framework. **(c)**: The illustration of our proposed framework. There are two image recon stages and one s-map estimation stage. Compared with SSDU framework, we incorporate the temporal basis $\mathbf{\Phi}$ into the image stage I_1 and reconstruct the coefficients $\boldsymbol{\alpha}$ of the basis instead of images. The temporal images $\hat{\mathbf{X}}_\mathbf{T}$ could be recovered by $\mathbf{\Phi}\boldsymbol{\alpha}$ and are used for the s-map estimation stage C_1 to estimate s-maps $\hat{S}$. The estimated s-maps $\hat{S}$ are used for the following image reconstruction stage I_2 with the subspace model as well. Note that we stop the gradient flow between stages by setting $\hat{\mathbf{X}}_\mathbf{T}$ and $\hat{\mathbf{S}}$ as constant.

ularization with a data consistency term using an unrolled iterative reconstruction algorithm (Aggarwal et al., 2018).

$$\mathbf{Z}^{(i-1)} = \mathcal{D}_{\mathbf{I}}\left(\mathbf{X}^{i-1}\right) \tag{2}$$

$$\mathbf{X}^{(i)} = \arg\min_{\mathbf{X}} \|\mathbf{Y} - \mathbf{MFSX}\|_2^2 + \mu \left\|\mathbf{X} - \mathbf{Z}^{(i-1)}\right\|_2^2 \tag{3}$$

$$= \left((\mathbf{MFS})^H (\mathbf{MFS}) + \mu\mathbf{I}\right)^{-1} \left((\mathbf{MFS})^H \mathbf{Y} + \mu\mathbf{Z}^{(i-1)}\right) \tag{4}$$

where $\mathcal{D}_{\mathbf{I}}$ is a trainable network as a regularization, $\mathbf{X}^{(i)}$ is the reconstructed image and $\mathbf{Z}^{(i-1)}$ is the slack variable at the i-th iteration. The closed-form solution to the data consistency step (Eq. 3) requires an infeasible matrix inversion. Instead, we use the Conjugate Gradients (CG) method to solve Eq. 4.

To learn the regularization function without access to fully-sampled ground truth, the self-supervised framework divides the acquired kspace Ω into two disjoint sub-kspaces $\Omega = \Theta \cup \Lambda$. The sub-kspace $\mathbf{Y}_\Theta$ is used for the data consistency term, i.e., $\mathbf{Y}$ and $\mathbf{M}$ are replaced by $\mathbf{Y}_\Theta$ and $\mathbf{M}_\Theta$ respectively. The other sub-kspace $\mathbf{Y}_\Lambda$ is used for computing the the normalized $l_1 - l_2$ loss $\mathcal{L}$ between $\mathbf{Y}_\Lambda$ and the predicted kspace $\mathbf{M}_\Lambda\mathbf{FS}\hat{\mathbf{X}}$ in the same Λ region for the network training, where $\hat{\mathbf{X}}$ is the output of the final unrolled block (Yaman et al., 2020b,a, 2021).

2.3. Proposed reconstruction method

Our proposed reconstruction method extends the self-supervised image reconstruction framework to incorporate the temporal subspace model and jointly estimate the sensitivity maps.

I. Zero-shot self-supervised image reconstruction with subspace model: While the self-supervised framework achieves impressive results for single-time point, structural imaging, it does not take into account temporal correlations when applied to time-resolved imaging. We incorporate the linear subspace model into the self-supervised framework to enable reconstruction of time-resolved MRI data with significantly reduced degrees of freedom and a learned regularization from under-sampled data.

$$\mathbf{Z}_{\mathbf{I}}^{(i-1)} = \mathcal{D}_{\mathbf{I}}\left(\boldsymbol{\alpha}^{i-1}\right) \tag{5}$$

$$\boldsymbol{\alpha}^{(i)} = \arg\min_{\boldsymbol{\alpha}} \|\mathbf{Y}_{T\Theta} - \mathbf{M}_\Theta\mathbf{FS}\boldsymbol{\Phi}\boldsymbol{\alpha}\|_2^2 + \mu_I \left\|\boldsymbol{\alpha} - \mathbf{Z}_{\mathbf{I}}^{(i-1)}\right\|_2^2 \tag{6}$$

where $\mathbf{Y}_{T\Theta}$ is the temporal kspace for the data consistency. We use the same $l_1 - l_2$ loss to update the parameters in the network as described above.

In addition, we apply our technique in a zero-shot fashion where we only have access to the under-sampled data to reconstruct. In order to mitigate overfitting, we randomly generate a new pair of disjoint masks for each training epoch (Quan et al., 2020).

The proposed framework requires much higher GPU memory for back-propagation related to the data consistency term due to the additional echo dimension. We use CG to approximate the gradient flow of the data consistency term, where

$$\left(\nabla_{\mathbf{Z}_{\mathbf{I}}^{(i-1)}}\mathcal{L}\right) = \left((\mathbf{M}_\Theta\mathbf{FS}\boldsymbol{\Phi})^H (\mathbf{M}_\Theta\mathbf{FS}\boldsymbol{\Phi}) + \mu_I\mathcal{I}\right)^{-1} \left(\nabla_{\boldsymbol{\alpha}^{(i)}}\mathcal{L}\right) \tag{7}$$

II. Self-supervised sensitivity map estimation: Standard algorithms, like ESPIRIT (Uecker et al., 2014), estimate coil sensitivity maps, $\mathbf{S}$, from fully sampled auto-calibration scans (ACS). To shorten total scan time or handle situations without pre-acquired sensitivity maps, we propose an unrolled self-supervised method to reconstruct sensitivity maps directly from the acquired FSE data.

$$\mathbf{Z}_{\mathbf{C}}^{(i-1)} = \mathcal{D}_{\mathbf{C}}\left(\mathbf{S}^{(i-1)}\right) \tag{8}$$

$$\mathbf{S}^{(i)} = \arg\min_{\mathbf{S}} \|\mathbf{Y}_{T\Theta} - \mathbf{M}_{\Theta}\mathbf{F}\mathbf{X}_{\mathbf{T}}\mathbf{S}\|_2^2 + \mu_C \left\|\mathbf{S} - \mathbf{Z}_{\mathbf{C}}^{(i-1)}\right\|_2^2 + \lambda_C \|\mathbf{D}\mathbf{S}\|_2^2 \tag{9}$$

where $\mathbf{X}_{\mathbf{T}}$ are the temporal images and $\mathbf{D}$ is the spatial gradient operator which imposes smoothness constraints on the reconstructed sensitivity map. $\mathcal{D}_{\mathbf{C}}$ is another trainable network. We switch the order of $\mathbf{X}_{\mathbf{T}}$ and $\mathbf{S}$ because of the element-wise product. Eq. 9 can still be solved by CG algorithm.

We found simultaneously reconstructing the images and sensitivity maps to be unstable and sensitive to initialization. Instead, as presented in Fig. 1, the image reconstruction stage I_i and the sensitivity map estimation stage C_i are trained stage-by-stage. In this work, we use two image stages and one s-map stage. Each stage is trained for N steps. Each image/sensitivity stage uses the results from the previous sensitivity/image stage while the first image stage applies sensitivity maps estimated from ESPIRIT, which utilizes the central k lines in the acquired FSE data. To avoid overfitting, the sampling mask for the blocks are generated randomly and independently. To further stabilize the reconstruction, we added the $l_1 - l_2$ loss as the intermediate loss for the sensitivity map estimation block and prevented gradient flow between the blocks.

3. Experiments and Results

3.1. Dataset

We evaluate our proposed reconstruction method on both simulated and retrospective in-vivo 2D FSE data. The FSE protocols are different between the simulated and the in-vivo data to show the generalization of our proposed method.

For the simulated data, the EPG algorithm simulates a FSE sequence with (8 coils, T=80 echoes, echo spacing of 5.56 ms, matrix size of 190×256 and 160° refocusing train) based on numerical brain T2 and proton density maps (Collins et al., 1998).

For the retrospective in-vivo data, we acquired a fully-sampled spatial-temporal multi-echo dataset on human brain (FOV=180mm×240mm, matrix size of 208×256, slice thickness=3mm, echo spacing=11.5ms, T=32 echoes, 12 coils) (Zhao et al., 2015).

3.2. Experimental setup

The EPG algorithm simulates a dictionary of FSE signal evolution with a T2 range of 5 - 400 ms, T1 = 1000 ms, and refocusing angle = 160, 180 for the simulated and in-vivo dataset respectively. Then, the SVD of the dictionary generates a basis for the subspace model with $K = 3$.

To generate T2-shuffling data, we under-sampled each echo in the simulated dataset by $R = 24$ (8 phase encoding lines/echo) and in the in-vivo dataset by $R = 16$ (13 phase encoding lines/echo). For the ESPIRIT, we sampled $\{2, 4, 6\}$ (simulated data) and $\{2, 4, 6, 8, 10\}$ (in-vivo data) phase encoding (ky) lines at the center of the kspace, while ensuring that the acceleration rate stayed at either R=24 or 16. To model a T2-shuffling acquisition, the non-calibration k-space lines were randomly distributed throughout the echo train.

For model training, we train the image stage I_1 for 100 steps, I_2 for 100 steps and the s-map stage C_1 for 100 steps with an Adam (Kingma and Ba, 2014) optimizer. For the image stage I_1, the learning rate is 5e-4 and 1e-4 for the simulated and retrospective experiments respectively (both decay to 5e-5 after 40 steps). For all experiments, we use 5e-5 for the image stage I_2 and 5e-5 for the s-map stage C_1, regularization parameters $\mu_I = 0.05$, $\mu_C = 0.02$ and $\lambda_C = 2.0$, and 10 unrolled block.

We compare four methods: 1) 2D T2 shuffling reconstruction (Shuffling), 2) SSDU with individual images (SSDU), 3) SSDU incorporated with the subspace model (Ours-sub) and 4) our proposed joint image and sensitivity map reconstruction with the subspace model (Ours-joint). We repeat each experiment 5 times to report the mean and variance of quantative metrics. For the Shuffling method, we choose l1-wavelet as the regularization (Iyer et al., 2021). All experiments are performed on a NVIDIA TESLA V100 for 40 mins.

3.3. Results

We evaluate performance by measuring the Normalized Mean Square Error (NMSE) and the Structural Similarity (SSIM) (Wang et al., 2004) of the reconstructed magnitude images and the NMSE of the estimated T2 maps, since FSE sequences yield echoes with constant phase.

Table 1: Mean NMSE (%) and SSIM of the reconstructed temporal images and estimated T2 maps with 2 center ky lines. NMSE-I and SSIM-I stand for the NMSE and SSIM of the images, NMSE-T2 stands for the NMSE of the T2 maps. $\star$ represents the presence of pre-acquired sensitivity maps. Sf stand for the Shuffling method.

Data	Metric	Sf$\star$	SSDU$\star$	Sub$\star$	Sf	Sub	Joint
3*Simulated	NMSE-I (%)	9.16	42.3	**7.23**	19.3	18.8	**11.2**
	SSIM-I	0.945	0.693	**0.964**	0.895	0.910	**0.942**
	NMSE-T2 (%)	24.7	35.5	**18.9**	29.7	26.6	**22.5**
3*In-vivo	NMSE-I (%)	16.2	35.1	**11.9**	19.5	17.2	**16.2**
	SSIM-I	0.942	0.840	**0.950**	0.922	0.924	**0.928**
	NMSE-T2 (%)	18.4	28.4	**17.3**	25.5	23.9	**21.4**

I. Simulated data Table 1 shows quantitative performance of the different methods with just two center ky lines, as this most closely represents a standard T2-shuffling acquisition. With pre-acquired coil-sensitivity maps, our proposed technique improves image NMSE and SSIM, and T2 NMSE in comparison to the baseline techniques. Without access

to sensitivity maps, the proposed joint estimation of images and sensitivity maps outperforms shuffling and the non-joint proposed algorithm in all metrics.

Fig. 2(a) displays example reconstructed temporal images and estimated T2-maps from the different techniques. Again, with pre-acquired sensitivity maps, the proposed technique yields images and T2-maps with lower NMSE, improved SSIM, and qualitatively less artifacts. Without sensitivity maps, the ESPIRIT algorithm produces maps that lead to signal bias. Our proposed joint reconstruction method estimates better sensitivity maps, leading to higher fidelity image reconstructions. Fig. 2(b) plots average SSIM and NMSE across all echoes for sampling patterns with different numbers of central k-space lines. Our proposed technique readily integrates with different sampling patterns and out-performs the baselines in all cases.

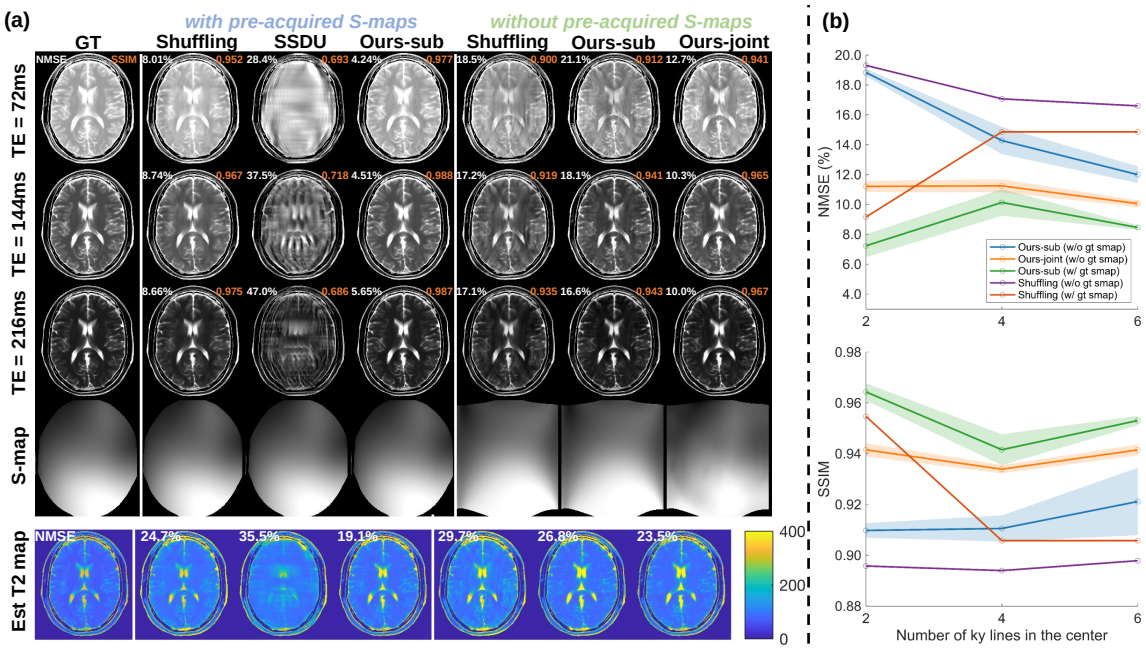

Figure 2: **(a)**: Examples of the reconstructed temporal images and estimated T2 maps on the simulated data with 2 center phase encoding lines. The NMSE and SSIM are calculated based on the magnitude of the images. To have a clear view of the details, we modify the lightness of the images. As SSDU fails to reconstruct the image, we only ran the experiment of SSDU once. **(b)**: The mean NMSE and SSIM of the reconstructed temporal images with different numbers of center phase encoding lines on the simulated data. The solid lines are the average metrics and the filled regions represent the value of the standard deviation (std) plus-minus of the metrics.

II. In-vivo data Table 1 and Fig. 3(a) show average performance metrics and reconstructed examples from the sampling pattern with 2 center ky lines in the in-vivo data. Even with imaging parameters that vary from the simulation experiments, the proposed methods outperform the compared methods quantitatively. Qualitatively, shuffling suffers from a

variety of artifacts while the proposed methods more closely resembles ground truth. Additionally, without pre-acquired sensitivity maps, the proposed joint reconstruction method produces images with improved NMSE and SSIM and less imaging artifacts.

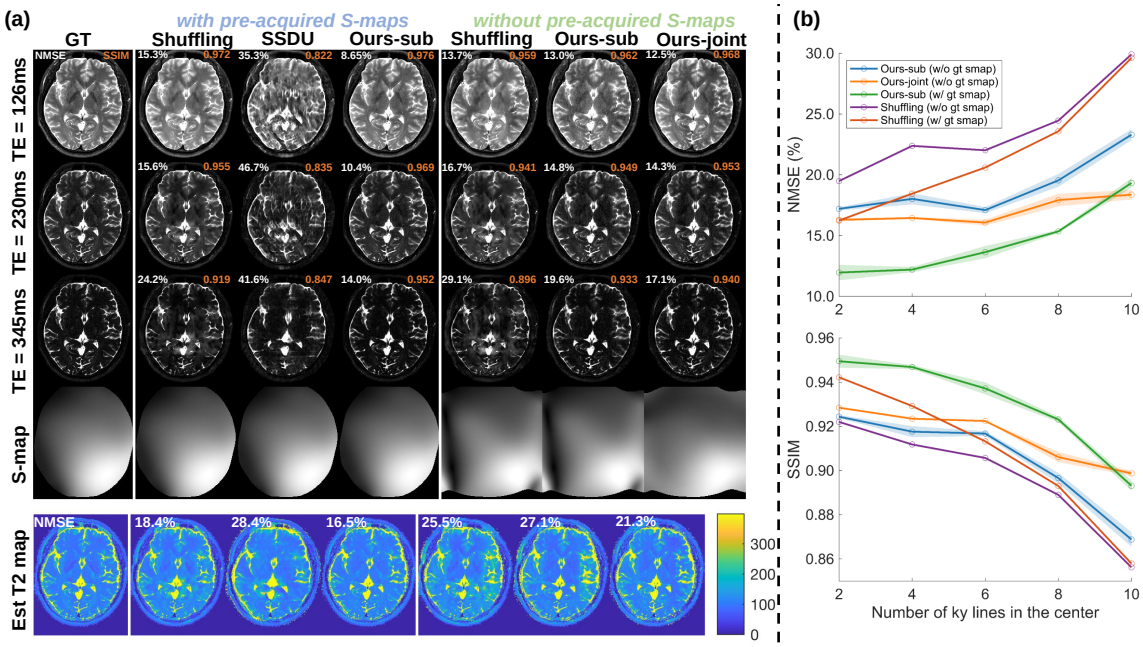

Figure 3: **(a)**: Examples of the reconstructed temporal images and estimated T2 maps on the in-vivo data with 2 center phase encoding lines. We also modify the lightness of the images to have a better view. SSDU is only run once. **(b)**: The mean NMSE and SSIM of the reconstructed temporal images with different numbers of center phase encoding lines on the in-vivo data.

As seen in Fig. 2(b) and 3(b), the proposed method outperforms the baselines with sampling patterns using various numbers of center ky lines. Notice that between the simulated and in-vivo dataset, a pattern does not necessarily exist between reconstruction performance and the number of center ky lines. Performance does not necessarily improve with more center ky lines as each sampling pattern uses the same overall acceleration rate, and the trade-off between center and external k-space lines for performance differs across various dataset.

4. Conclusion

In this work we proposed a novel zero-shot self-supervised method for time-resolved MRI reconstruction from 2D FSE acquisitions. Our proposed approach incorporates the temporal subspace model into the existing self-supervised reconstruction framework to simultaneously learn a regularization function from the under-sampled data itself and exploit temporal correlations to significantly reduce degrees of freedom in the reconstruction. Moreover, a

self-supervised sensitivity estimation stage is proposed which only utilizes the acquired data to further shorten the total scanning time.

Future work could extend our framework to dynamic image reconstruction where a motion model will replace the signal model used in this work. In addition, the joint reconstruction of dynamic sensitivity maps and dynamic images could improve performance in comparison to using static, pre-acquired sensitivity maps which do not account for motion.

References

Hemant K Aggarwal, Merry P Mani, and Mathews Jacob. Modl: Model-based deep learning architecture for inverse problems. *IEEE transactions on medical imaging*, 38(2):394–405, 2018.

Marius Arvinte, Sriram Vishwanath, Ahmed H Tewfik, and Jonathan I Tamir. Deep j-sense: Accelerated mri reconstruction via unrolled alternating optimization. In *International Conference on Medical Image Computing and Computer-Assisted Intervention*, pages 350–360. Springer, 2021.

Shanshan Bao, Jonathan I Tamir, Jeffrey L Young, Umar Tariq, Martin Uecker, Peng Lai, Weitian Chen, Michael Lustig, and Shreyas S Vasanawala. Fast comprehensive single-sequence four-dimensional pediatric knee mri with t2 shuffling. *Journal of Magnetic Resonance Imaging*, 45(6):1700–1711, 2017.

Noam Ben-Eliezer, Daniel K Sodickson, and Kai Tobias Block. Rapid and accurate t2 mapping from multi–spin-echo data using bloch-simulation-based reconstruction. *Magnetic resonance in medicine*, 73(2):809–817, 2015.

D Louis Collins, Alex P Zijdenbos, Vasken Kollokian, John G Sled, Noor J Kabani, Colin J Holmes, and Alan C Evans. Design and construction of a realistic digital brain phantom. *IEEE transactions on medical imaging*, 17(3):463–468, 1998.

Juergen Hennig. Multiecho imaging sequences with low refocusing flip angles. *Journal of magnetic Resonance (1969)*, 78(3):397–407, 1988.

Jürgen Hennig, A Nauerth, and HRARE Friedburg. Rare imaging: a fast imaging method for clinical mr. *Magnetic resonance in medicine*, 3(6):823–833, 1986.

Siddharth Iyer, Daniel Polak, Congyu Liao, Jonathan I Tamir, Stephen F Cauley, Borjan Gagoski, Wei-Ching Lo, Berkin Bilgic, and Kawin Setsompop. Wave-encoding and shuffling enables rapid time resolved structural imaging. *arXiv preprint arXiv:2103.15881*, 2021.

Yohan Jun, Hyungseob Shin, Taejoon Eo, and Dosik Hwang. Joint deep model-based mr image and coil sensitivity reconstruction network (joint-icnet) for fast mri. In *Proceedings of the IEEE/CVF Conference on Computer Vision and Pattern Recognition*, pages 5270–5279, 2021.

Diederik P Kingma and Jimmy Ba. Adam: A method for stochastic optimization. *arXiv preprint arXiv:1412.6980*, 2014.

Michael Lustig, David L Donoho, Juan M Santos, and John M Pauly. Compressed sensing mri. *IEEE signal processing magazine*, 25(2):72–82, 2008.

John P Mugler III. Optimized three-dimensional fast-spin-echo mri. *Journal of magnetic resonance imaging*, 39(4):745–767, 2014.

Yuhui Quan, Mingqin Chen, Tongyao Pang, and Hui Ji. Self2self with dropout: Learning self-supervised denoising from single image. In *Proceedings of the IEEE/CVF conference on computer vision and pattern recognition*, pages 1890–1898, 2020.

Jonathan I Tamir, Martin Uecker, Weitian Chen, Peng Lai, Marcus T Alley, Shreyas S Vasanawala, and Michael Lustig. T2 shuffling: sharp, multicontrast, volumetric fast spin-echo imaging. *Magnetic resonance in medicine*, 77(1):180–195, 2017.

Martin Uecker, Peng Lai, Mark J Murphy, Patrick Virtue, Michael Elad, John M Pauly, Shreyas S Vasanawala, and Michael Lustig. Espirit—an eigenvalue approach to autocalibrating parallel mri: where sense meets grappa. *Magnetic resonance in medicine*, 71(3): 990–1001, 2014.

Zhou Wang, Alan C Bovik, Hamid R Sheikh, and Eero P Simoncelli. Image quality assessment: from error visibility to structural similarity. *IEEE transactions on image processing*, 13(4):600–612, 2004.

Burhaneddin Yaman, Seyed Amir Hossein Hosseini, Steen Moeller, Jutta Ellermann, Kâmil Uğurbil, and Mehmet Akçakaya. Multi-mask self-supervised learning for physics-guided neural networks in highly accelerated mri. *arXiv preprint arXiv:2008.06029*, 2020a.

Burhaneddin Yaman, Seyed Amir Hossein Hosseini, Steen Moeller, Jutta Ellermann, Kâmil Uğurbil, and Mehmet Akçakaya. Self-supervised learning of physics-guided reconstruction neural networks without fully sampled reference data. *Magnetic resonance in medicine*, 84(6):3172–3191, 2020b.

Burhaneddin Yaman, Seyed Amir Hossein Hosseini, and Mehmet Akçakaya. Zero-shot self-supervised learning for mri reconstruction. *arXiv preprint arXiv:2102.07737*, 2021.

Bo Zhao, Wenmiao Lu, T Kevin Hitchens, Fan Lam, Chien Ho, and Zhi-Pei Liang. Accelerated mr parameter mapping with low-rank and sparsity constraints. *Magnetic resonance in medicine*, 74(2):489–498, 2015.

(10)